RSC Advances

PAPER

View Article Online
View Journal | View Issue

Cite this: *RSC Adv.*, 2017, **7**, 20851

Surface patterning of single-walled carbon nanotubes enhances their perturbation on a pulmonary surfactant monolayer: frustrated translocation and bilayer vesiculation†

Tongtao Yue, ‡*[a] Yan Xu,‡[a] Shixin Li,[a] Zhen Luo,[a] Xianren Zhang [b] and Fang Huang[a]

The pulmonary surfactant monolayer (PSM) is a complex material lining the air–water interface of lung alveoli to avoid its collapse by reducing surface tension. Once external particles are inhaled and captured by the PSM, this property might be perturbed to induce inhalation toxicity. However, relatively little is known regarding the detailed interaction between inhaled particles and the PSM. Here, by applying the coarse-grained molecular dynamics simulation method, we probe how inhaled single-walled carbon nanotubes (SWCNTs) interact with the PSM. For pristine SWCNTs, they are found to insert into or be wrapped by the PSM, depending on the tube size and the PSM tension. For hydrophilic tubes, they spontaneously translocate across the PSM, regardless of the tension. In contrast to SWCNTs with unique surface properties, the surface patterning of SWCNTs enhances their perturbation on the PSM. Under expansion, the PSM translocation is frustrated *via* inducing the ordered or disordered lipid arrangement adhering to the patterned tube surface. Under compression, the lipid rearrangements further self-adjust and grow into bilayers, which protrude along the tube surface and finally develop into vesicles. The stripe width and stripe orientation, among other factors, are found to be the most important factors that determine whether and how the vesiculation takes place.

Received 3rd February 2017
Accepted 5th April 2017

DOI: 10.1039/c7ra01392b

rsc.li/rsc-advances

1. Introduction

In the lungs, the branching airways end with small alveoli, which are covered by a thin film of lung surfactant, called the pulmonary surfactant monolayer (PSM).[1] Apart from host defense, the major biophysical function of the PSM is to reduce the tension of the air–water interface by 2D phase transition and 3D shape transformation.[2–5] In particular, under deep expiration, the PSM becomes unstable at the interface and collapses. This is characterized by a loss of material from the interface and can proceed through different pathways: lipid bilayer folding and reconstruction *via* formation of higher ordered structures, like vesicles, twisted ribbons and giant folds.[6] All these structures can be seen as lipid reservoirs which are crucial for maintaining low surface tension by transferring material between the monolayer and the reservoirs.[7–9] This material recycling is facilitated by the SP-B and SP-C proteins, which help maintain the monolayer–reservoir connectivity.[10,11]

During respiration, external fine particles, especially the nanoparticles (NPs), can be inhaled and first captured by the PSM. It is expected that the detailed interactions of inhaled NPs with the PSM influence their subsequent fate and, adversely, cause severe PSM damage, which further leads to the enhanced susceptibility to pathological conditions, like asthma, respiratory distress syndrome and pulmonary inflammation.[12–14] Having known how the PSM plays biophysical functions, it becomes urgent to elucidate how the inhaled NPs perturb the ultrastructure of the PSM and, especially, frustrate its normal shape transformation.

Single-walled carbon nanotubes (SWCNTs) have attracted considerable industrial attention due to their inimitable physicochemical properties, which suggest possible applications in different areas of science and technology.[15–18] The large scale production containing SWCNTs may lead to the environmental release and the accidental exposure during manufacture, use, or disposal of the products. Although inhalation of SWCNTs may cause adverse impact,[19] relatively little is known about the mechanism of their pulmonary entry, which is an important consideration in the pulmonary nanodrug delivery.[20–22] Inspired by above facts and considerations, it is thus of quite importance

[a]*State Key Laboratory of Heavy Oil Processing, Center for Bioengineering and Biotechnology, College of Chemical Engineering, China University of Petroleum (East China), Qingdao, 266580, China. E-mail: yuett@upc.edu.cn*

[b]*State Key Laboratory of Organic–Inorganic Composites, College of Chemical Engineering, Beijing University of Chemical Technology, Beijing, 100029, China*

† Electronic supplementary information (ESI) available. See DOI: 10.1039/c7ra01392b

‡ These authors contributed equally to the work.

to systematically investigate the detailed interactions between inhaled SWCNTs and the PSM.

In our previous study, we explored how the pristine SWCNT size and PSM tension cooperate to modulate their interactions. Four different interaction states, including the vertical insertion, the PSM poration, the lipid extraction and the SWCNT encapsulation, were identified. In practical applications, however, SWCNTs may not have homogeneous surface properties but display distinct regular or irregular patterning. Or, it can be designed to be patterning to improve the delivery efficiency and reduce the side effects during translocation across the cell membranes. It has been widely accepted that the hydrophobicity of NPs, including the SWCNTs, plays critical roles in their interactions with lipid membranes. For example, Verma *et al.* investigated the cell membrane penetration of NPs with three different surface structures.[23] They showed that the NPs decorated with subnanometre striations of alternating anionic and hydrophobic groups penetrate the membrane with less bilayer disruption. For SWCNTs, similarly, it has been experimentally observed that the surface functionalization of SWCNTs can enhance their penetration through the cell membrane.[24] This observation was confirmed by theoretical investigations, which suggested that certain patterning of SWCNTs can reduce the system free energy as they traverse through the lipid bilayer.[25] Based on the existing similar researches,[23,26] we surmise that both PSM translocation and PSM perturbation of surface patterned SWCNTs should be different to those of pristine SWCNTs because of the ordered or disordered arrangements of hydrophilic and hydrophobic surface properties. In this work, we conducted the coarse-grained molecular dynamics (CGMD) simulations to elucidate how the surface patterning of SWCNTs influences their interactions with the PSM, mainly focusing on the PSM perturbation and the internalization pathway.

2. Models and simulation methods

2.1. PSM model

The composition of real PSM is quite complex. By weight, lipids account for about 90% of the surfactant while proteins make up the other 10%. Among the lipids, the most abundant component is dipalmitoylphosphatidylcholine (DPPC), along with a few other phosphatidylcholine (PC), phosphatidylglycerol (PG) and cholesterol.[27–30] Four kinds of proteins, including SP-A, SP-B, SP-C, and SP-D, are associated with the PSM and responsible for different functions.[31–33] In this work, we prepared the model PSM by constructing two symmetric DPPC monolayers, each consisting 5102 DPPC lipids, and 368 793 water particles in total (Fig. S1a†). The choice of DPPC is because it is the major component of PSM and responsible for reduction of surface tension in the lungs to near zero.[34]

2.2. SWCNT model

The honeycomb structure of SWCNT was reduced to a triangular lattice structure, where every three carbons in the all-atom SWCNT were modeled as one particle (Fig. S1b†). To systematically investigate the influence of surface patterning of SWCNTs on their interactions with the PSM, four types of nanotubes were prepared by varying both bead type and bead arrangement: (1) hydrophobic (pristine) SWCNTs with C1 type beads (C1 is the Martini parameter representing the hydrophobic property); (2) hydrophilic (oxidized) SWCNTs with Nda type beads (Nda represents the hydrophilic property); (3) stripy SWCNTs with alternating C1 and Nda type beads; (4) SWCNTs with random distribution of C1 and Nda type beads. For the stripy SWCNTs, both tangential and axial stripes were designed for comparison. To maintain both the tubular structure and normal mechanical property of SWCNTs, the angular force constant and equilibrium angle along axial direction are $\kappa_{\text{angle}} = 700$ kcal mol^{-1} rad^{-2} and $\theta = 60^{\circ}$. Along tangential direction, the equilibrium angle is not constant but determined by the tube diameter. The bond force constant and equilibrium bond length are $\kappa_{\text{bond}} = 700$ kcal mol^{-1} and $l = 0.3684$ nm. The dihedral angle force constant, multiplicity, and equilibrium angle are $\kappa_{\chi} = 3.1$ k cal mol^{-1}, $n = 2$, and $\delta = 180^{\circ}$. The specific CG model as well as parameters comes from the previous simulation work of Titov *et al.*, and has been successfully used to simulate interaction between graphene nanosheets and lipid bilayer and lipid monolayer.[35,36]

2.3. Simulation details

CGMD simulations were performed using the GROMACS software package (v.4.6.7).[37] The Martini force field was used for all simulations.[38] In all simulations, the SWCNTs were placed initially in vacuum above the DPPC monolayer. After energy minimization, CGMD simulations with constant particle number, surface tension and temperature were performed. For all non-bonded interactions, the standard cutoffs for the CG force field were used: the Lennard-Jones potential was smoothly shifted to zero between 0.9 nm and 1.2 nm to reduce the cutoff noise, whereas the coulomb potential, with a cutoff of 1.2 nm, was smoothly shifted to zero from 0 nm to 1.2 nm. Temperature was kept at 310 K using the Berendsen weak coupling algorithm with a time constant of 2.5 ps. The Berendsen algorithm was applied for constant surface tension to imitate the inspiration and expiration conditions. The system compressibility was set to 5×10^{-5} bar^{-1} in the lateral direction and 0 bar^{-1} in the normal direction. The neighboring list for non-bonded interactions was updated every 10 steps. Snapshots of the simulation system in the paper were rendered by VMD.[39]

3. Results and discussion

3.1. Pristine SWCNTs

We started our simulations to preliminarily examine how the pristine SWCNTs interact with the PSM. To model different respiration conditions, we fixed the surface tension to 30 mN m^{-1} and 10 mN m^{-1}, respectively.[40,41] MD simulations suggested that the pristine SWCNTs can insert into, translocate across or be wrapped by the PSM, depending on the tube size and PSM tension. Specially, ultrashort SWCNTs with lengths comparable to the monolayer thickness ($L = 1.25$ nm) were

found to vertically insert into the PSM, regardless of the PSM tension (Fig. 1a and e). However, a slight increase of tube length ($L = 4.47$ nm) caused distinct interaction pathways, depending on the PSM tension. Under expansion (30 mN m^{-1}), the SWCNT was found to insert into the PSM and opened a hydrophilic pore *via* structural lipid rearrangement inside the tube (Fig. 1b). Under compression (10 mN m^{-1}), strikingly, it was encapsulated in PSM *via* shape transformation (Fig. 1f). For longer SWCNTs ($L = 14.04$ nm), they anchored into the PSM under expansion, being featured with the lipid extraction and the inverse micelle assembly covering the tube surface (Fig. 1c and d). Under compression, again, they can be wrapped by the PSM, but with the final entry angle that was controlled by the tube diameter (Fig. 1g and h).

3.2. Spontaneous translocation of hydrophilic SWCNTs across the PSM

To understand how the hydrophobicity of a nanotube influences its interaction with the PSM, we set the SWCNT to be hydrophilic by simply replacing the C1 type bead with Nda. Similar with the spherical NPs,[42,43] nearly all the hydrophilic nanotubes spontaneously translocated across the PSM, yet both the translocation pathway and the accompanied PSM perturbation were affected by the tube size and the PSM tension (Fig. 2). Under expansion (30 mN m^{-1}), all the nanotubes were found to translocate across the PSM, after which longer tubes horizontally adhered on the monolayer–water interface (Fig. 2a and b), while shorter ones maintained their vertical orientation (Fig. 2c and d). No obvious PSM perturbation was observed during the translocation process. Under compression (10 mN m^{-1}), the translocation was occasionally accompanied with complex shape transformation of the PSM (Fig. 2e–g). One exception was for the ultrashort SWCNT which was trapped on the monolayer–air interface without further translocation (Fig. 2h). Note that the similar trapping behaviors of solid rod-like NPs in PSM were reported recently by Lin *et al.*[44] As will be discussed below, the failure of penetration was mainly ascribed to the mild perturbation of PSM by ultrashort SWCNTs. Besides, the denser lipid packing under PSM compression further restrained the opening of physical defect, thus hindering the penetration of ultrashort SWCNTs through the PSM.

We choose the SWCNT with diameter of 3.52 nm and length of 14.04 nm to analyze a typical simulated translocation event under PSM compression. MD simulations suggested that it was the high aspect ratio of the SWCNT that facilitated its penetration through the monolayer, similar to a 'nanosyringe', as has been experimentally reported[24] and theoretically simulated[45] when interacting with a lipid bilayer. Combining the typical snapshots (Fig. 3a–c), the time evolution of interaction energy between tube and lipids (Fig. 3d), and that of the tube orientation angle (Fig. 3e), we describe the translocation mechanism by several successive stages. The first stage was featured with random translation and rotation of SWCNT before contact with the PSM. Once captured by PSM, the landing was accomplished rapidly *via* a fast self-rotating, corresponding to the first striking decrease of both the tube orientation angle and the interaction energy (Fig. 3d and e). In this stage, several lipids diffused into one mouth of the SWCNT (Fig. 3b), thus generating a structural defect, from which the SWCNT slightly tilted and rapidly acted as a 'syringe' to penetrate through the PSM *via* the tip first mechanism.[46–49] Simultaneously, lipid molecules beneath the tube rearranged themselves to initiate a folding transition. After translocation, this folding further grew under compression and finally developed into a disc-like lipid aggregate, with one tube mouth inserting into it (Fig. 3c). A similar shape transformation of the PSM *via* interacting with spherical NPs has been reported recently, where the SP-B proteins were found to participate in it.[43] Compared with the well-organized shape transformation of natural PSM under compression,[50] the passive bilayer folding initiated by penetration of hydrophilic SWCNTs might be adverse and inhibit the normal bio-function of the PSM.

For shorter hydrophilic nanotubes ($D = 5.28$ nm, $L = 4.47$ nm), they were found to directly translocate across the PSM under expansion with no apparent PSM perturbation (Fig. 2c). Under compression, however, a severe perturbation was observed (Fig. 4a). After penetrating through PSM *via* a fast self-rotating (Fig. 4b), similarly, a small protrusion was generated and plugged into one tube mouth ($t = 7$ ns). Interestingly, the protruding did not terminate but developed into a folding bilayer, the growth of which drove further tube rotation from

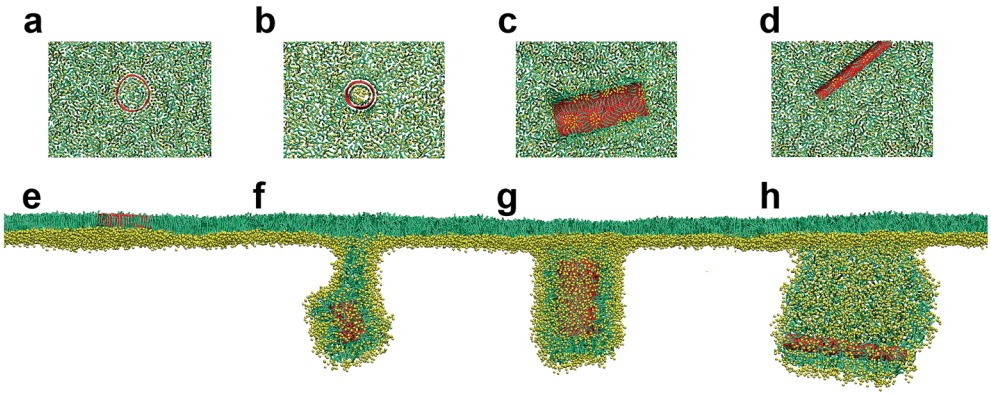

Fig. 1 Size dependent PSM interaction of pristine SWCNTs under both expansion (a–d) and compression (e–h). The SWCNT size was $L = 1.25$ nm, $D = 5.28$ nm (a and e); $L = 4.47$ nm, $D = 3.52$ nm (b and f); $L = 14.04$ nm, $D = 5.28$ nm (c and g); and $L = 14.04$ nm, $D = 1.76$ nm (d and h).

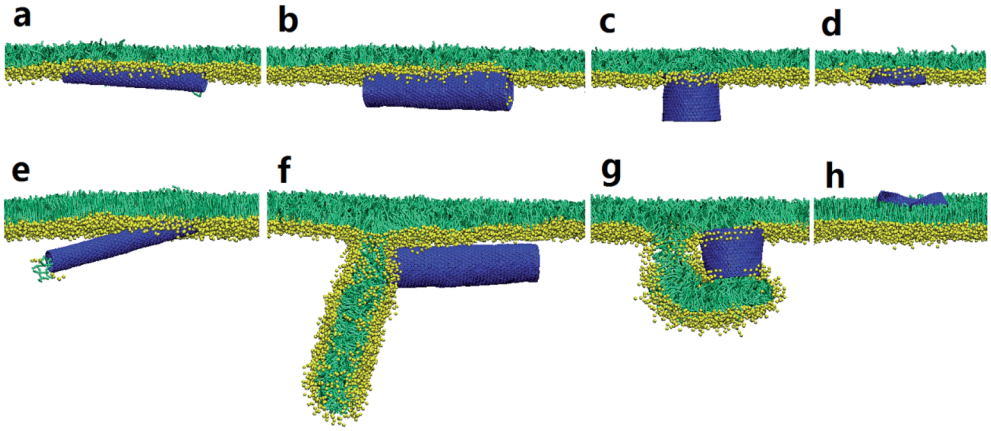

Fig. 2 Direct translocation of hydrophilic SWCNTs across the PSM. Both diameters and lengths of SWCNTs are: (a and e), $D = 1.76$ nm, $L = 14.04$ nm; (b and f), $D = 3.52$ nm, $L = 14.04$ nm; (c and g), $D = 5.28$ nm, $L = 4.47$ nm; (d and h), $D = 5.28$ nm, $L = 1.28$ nm. The PSM tension was fixed to 30 mN m^{-1} and 10 mN m^{-1} to model both expansion (a–d) and compression (e–h) conditions.

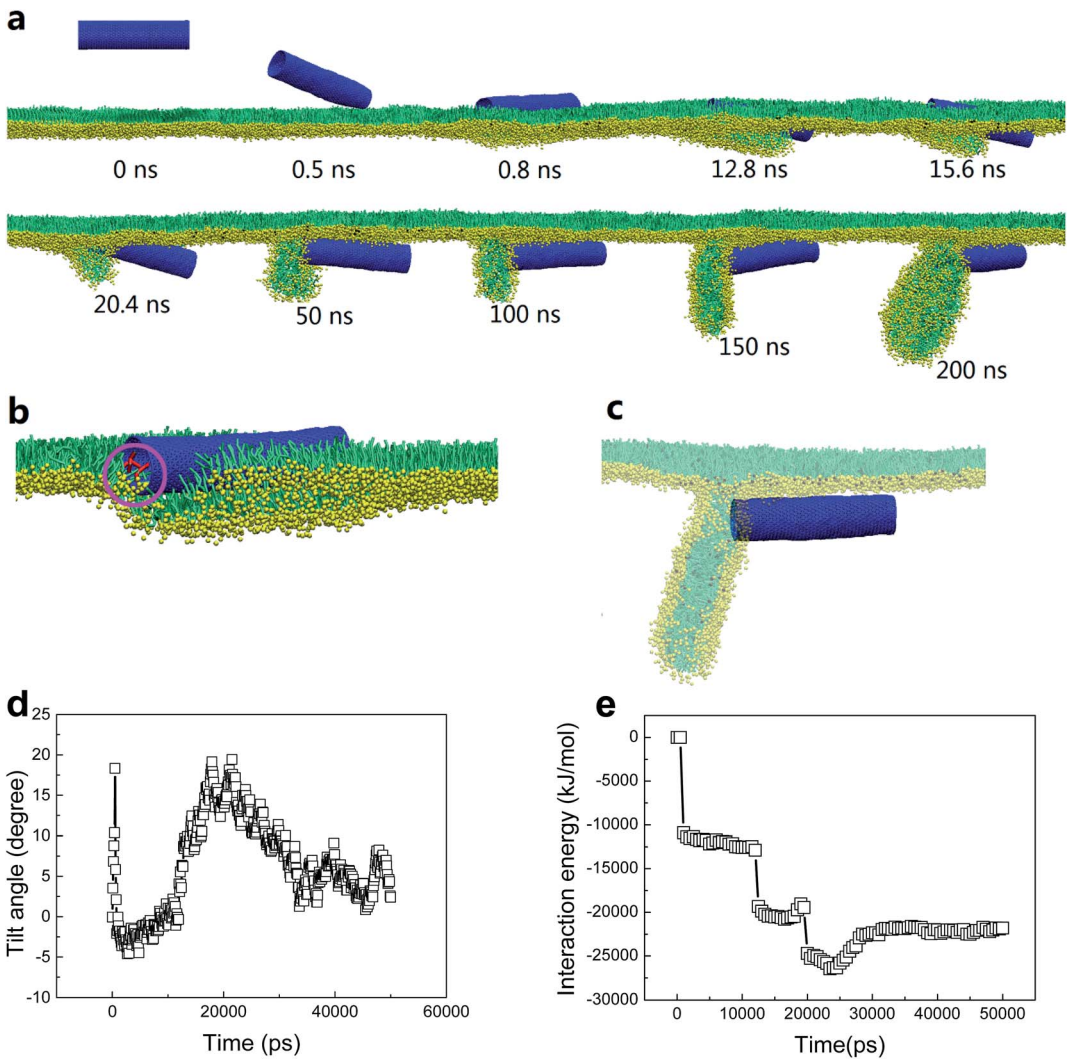

Fig. 3 (a) A typical simulated translocation event for a hydrophilic nanotube with diameter of 3.52 nm and length of 14.04 nm. (b) Instantaneous configuration illustrating the local lipids that diffused into nanotube to open a structural defect, from which the penetration is initiated. (c) The final configuration where lipids were set to be transparent to illustrate the anchorage of one tube mouth into the folding bilayer. (d) Time evolution of tilt angle of SWCNT during translocation process. (e) Time evolution of interaction energy between SWCNT and lipids. The PSM tension was fixed to 10 mN m^{-1}.

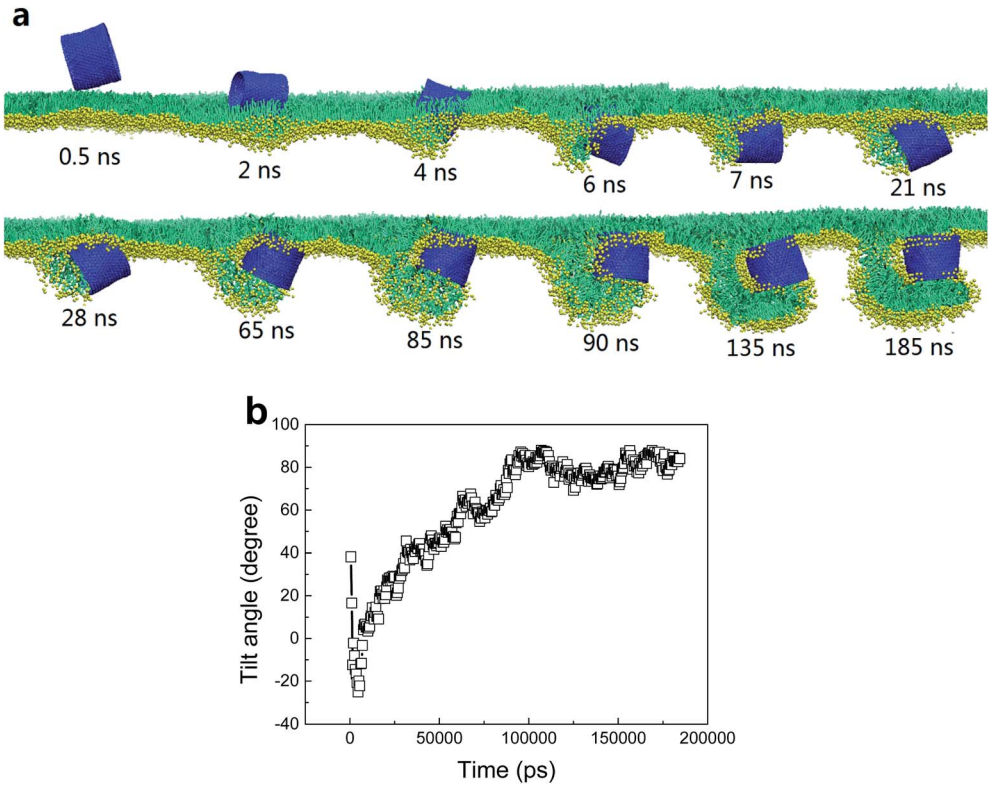

Fig. 4 (a) A typical simulated translocation event of a hydrophilic SWCNT with diameter of 5.28 nm and length of 4.47 nm. (b) Time evolution of tilt angle of SWCNT during translocation process. The PSM tension was fixed to 10 mN m^{-1}.

horizontal back to the vertical orientation (Fig. 4b). Finally, the tube was partially wrapped, with two ends anchoring into the curved folding bilayer and the upper monolayer.

Besides the tube size effect, further extensive simulations illuminated the importance of random entry angle in both translocation and PSM perturbation. We first take the SWCNT

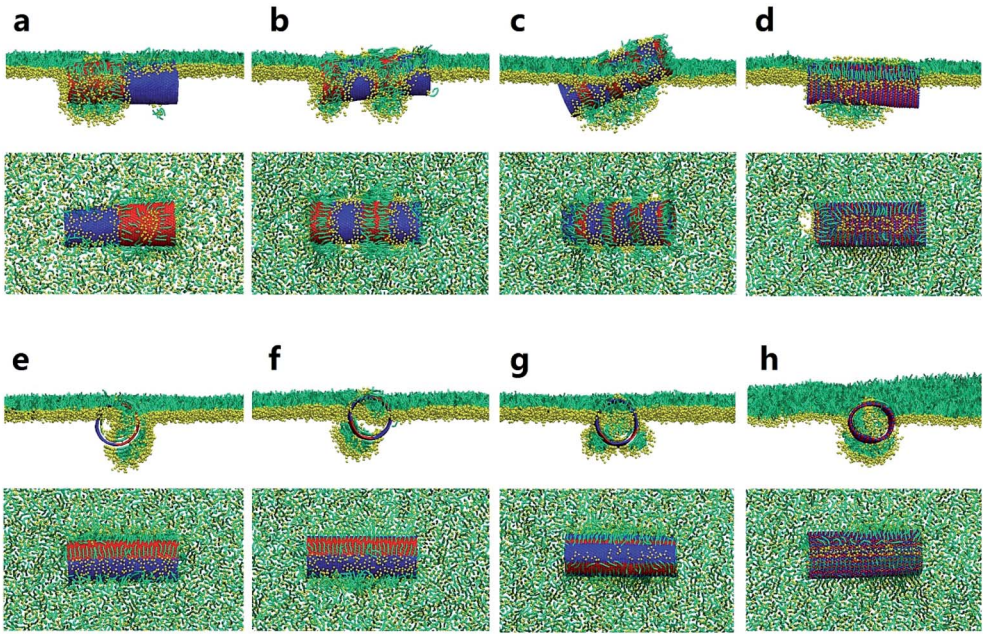

Fig. 5 Final configurations of PSM interaction of SWCNTs having tangential (a–d) and axial (e–h) stripes. All SWCNTs have the same size of L = 14.04 nm and D = 5.28 nm. The stripe width was varied by changing the number of stripes: 2 (a and e), 4 (b and f), 8 (c and g) and 45 (d and h). The PSM tension was fixed to 30 mN m^{-1}. Both top and side views of each configuration were provided for clarity.

with size of $L = 14.04$ nm and $D = 3.52$ nm as an example. Our repeat simulation revealed a distinct interaction pathway, where the SWCNT directly penetrated through the PSM without formation of the folding bilayer (Fig. S2a†). By comparing the evolutions of tube orientation angle (Fig. S2b†), we speculate that it was the tilt angle of SWCNT being captured by the PSM that influenced its subsequent translocation and accompanied PSM perturbation. Specifically, larger tilt angle (close to vertical orientation) of the SWCNT can facilitate its translocation since it has the minimum contact area with lipids.[25,47] If the SWCNT is captured by the PSM in a small tilt angle (close to horizontal orientation), the large contact area would induce a severe lipid rearrangement, which is requisite to the generation of folding bilayer or a higher dimensional shape transformation. For shorter SWCNT ($L = 4.47$ nm), similarly, different interaction pathways were observed (Fig. S3†). Generally, once captured by the PSM, it first flips on the monolayer surface to find or open a defect to initiate the subsequent penetration (Fig. S3a†). Otherwise, the translocation is failed and the tube would be trapped on the monolayer surface for a long time (Fig. S3b†). After translocation, both nature and extent of PSM perturbation could also be different. Similarly, the PSM perturbation should be reduced by increasing the entry angle of SWCNT. Though a slight protruding event was initiated both inside and outside the tube, interestingly, it rapidly recovered back to the monolayer, leaving the penetrated SWCNT standing with one mouth embedding in the monolayer (Fig. S3c†).

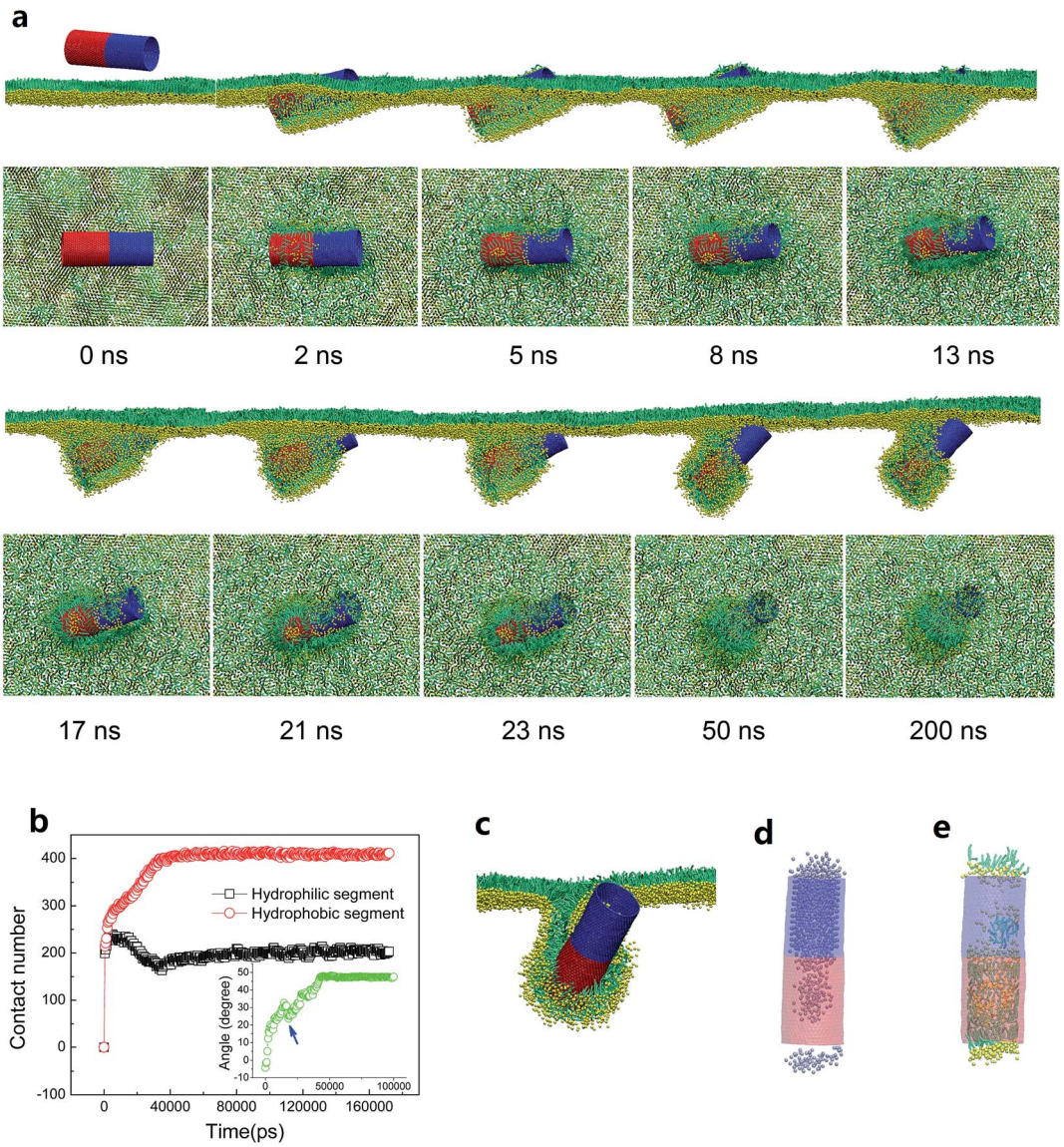

Fig. 6 PSM interaction of the SWCNT having two tangential stripes under compression. (a) Typical snapshots from both side and top views revealing the interaction mechanism that featured with half wrapping and half translocation. (b) Time evolutions of lipid number contacting with hydrophobic (red) and hydrophilic (black) segments of SWCNT. The inset shows the evolution of tilt angle of SWCNT. (c) Cross sectional view of the final configuration. (d) Water beads inside the SWCNT. (e) Inner lipid arrangement of SWCNT. The SWCNT size was $D = 5.28$ nm and $L = 14.04$ nm. The PSM tension was fixed to 10 mN m^{-1}.

3.3. Surface patterning of SWCNTs frustrates their translocation across the PSM under expansion

Above simulations have indicated that SWCNTs with the unique surface properties interact with the PSM *via* mechanisms that depend on the homogeneous surface hydrophobicity. While hydrophilic tubes spontaneously translocate across the PSM, hydrophobic tubes insert into, translocate across or are wrapped by the PSM, depending on the tube size and the PSM tension. Considering that the surface patterning of SWCNTs is prevalent and can be easily generated in reality *via* both surface self-assembly and covalent modification, we next investigate how the surface patterning of SWCNTs affects their interactions with the PSM. In fact, it has been observed that regular surface patterning of SWCNTs can enhance their penetration through a cell membrane,[25] and can reduce the membrane damage compared with no or other types of modification.[23,26,51] However, the case should be different for the PSM system due to the monolayer structure and striking asymmetry at the interface.

Here, we distinguished two types of stripes decorating the tube surface. One is along tangential direction and the other is along axial direction (Fig. S1b†). For each type, four SWCNTs with the same size (L = 14.04 nm, D = 5.28 nm) but different stripe widths were constructed. Surface tension of the PSM was fixed to 30 mN m^{-1} to model the expansion condition. The equilibrium configurations from both top and side views are given in Fig. 5, which shows that the PSM translocation of SWCNTs was frustrated by surface patterning. For the SWCNT having two tangential stripes, the interaction was featured with a half wrapping and half translocation mechanism (Fig. 5a).[52] While the hydrophilic segment directly translocated across the PSM, the hydrophobic segment was wrapped by lipids to protect it from water. To further decrease the interactive free energy, several lipid molecules were extracted from the PSM and formed inverse micelles covering the top surface of the tube.[53] For SWCNTs having four stripes, similarly, the hydrophilic stripes were immerged in water, leaving the hydrophobic parts covered by lipid aggregates, thus trapping the tube at the interface (Fig. 5b). Note that lipids adhering on the tube surface organized regularly with tails arranging along axial direction and heads facing towards the hydrophilic surface, so the configuration was analogous to a 'bilayer' distribution. As we further decreased the stripe width, the 'monolayer' rather than the 'bilayer' lipid arrangement covering the patterned tube surface was observed (Fig. 5c). The reduced order of lipid arrangement further frustrated the PSM translocation. For SWCNTs decorated with extremely narrow stripes, lipids were

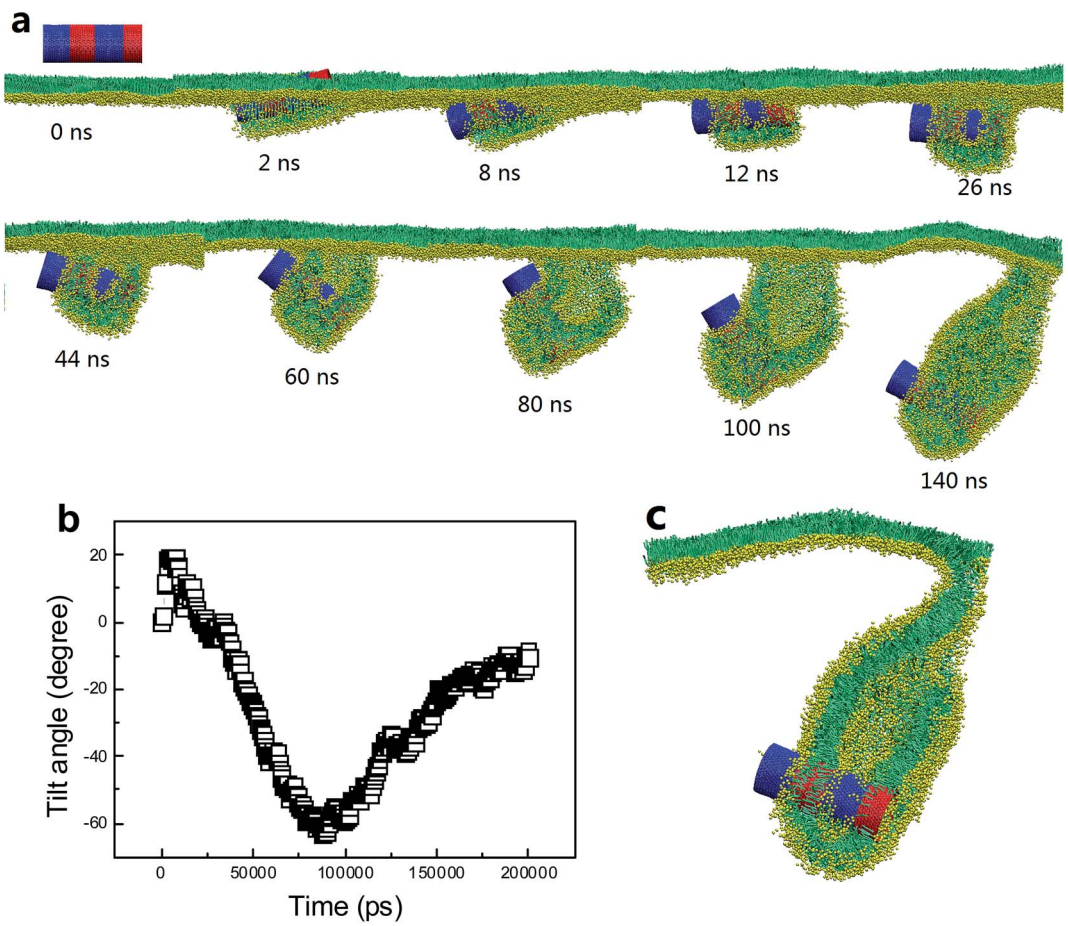

Fig. 7 PSM vesiculation *via* interacting with a SWCNT having four tangential stripes. (a) Typical snapshots showing the detailed vesiculation pathway. (b) Time evolution of tilt angle of SWCNT. (c) Cross sectional view of the final configuration revealing that two hydrophobic bands anchored themselves into the bilayer walls to stabilize the vesicle.

further confused and the assembly was more like a banded micelle, with tails arranging along the tangential direction (Fig. 5d). The final configurations for axial striped SWCNTs show the similar results that ordered or disordered lipid arrangement adhering on the patterned tube surface frustrated the translocation (Fig. 5e–h).

3.4. Surface patterning of SWCNTs causes bilayer vesiculation of the PSM under compression

Consider then what is different under compression. It has been known that PSM undergoes well-organized 2D phase transition or 3D shape transformation, like bilayer folding and twisting, to maintain low tension at the air–water interface. Based on the above results, we surmise that the normal shape transformation of the PSM under deep compression might be perturbed by interacting with surface patterned SWCNTs. Here, by varying the stripe width, a general interaction mechanism featured with inserting, rotating and lipid protruding, was identified. Strikingly, different stripe widths and stripe orientations, among other factors, were found to generate entirely different configurations.

We first look the SWCNT having two tangential stripes (Fig. 6). Multiple repeat simulations showed that the hydrophobic segment of SWCNT first contacted with and inserted into the PSM, leaving the hydrophilic segment lagged behind and temporarily exposed in vacuum (Fig. 6a). Several lipid molecules were extracted from the PSM and formed inverse

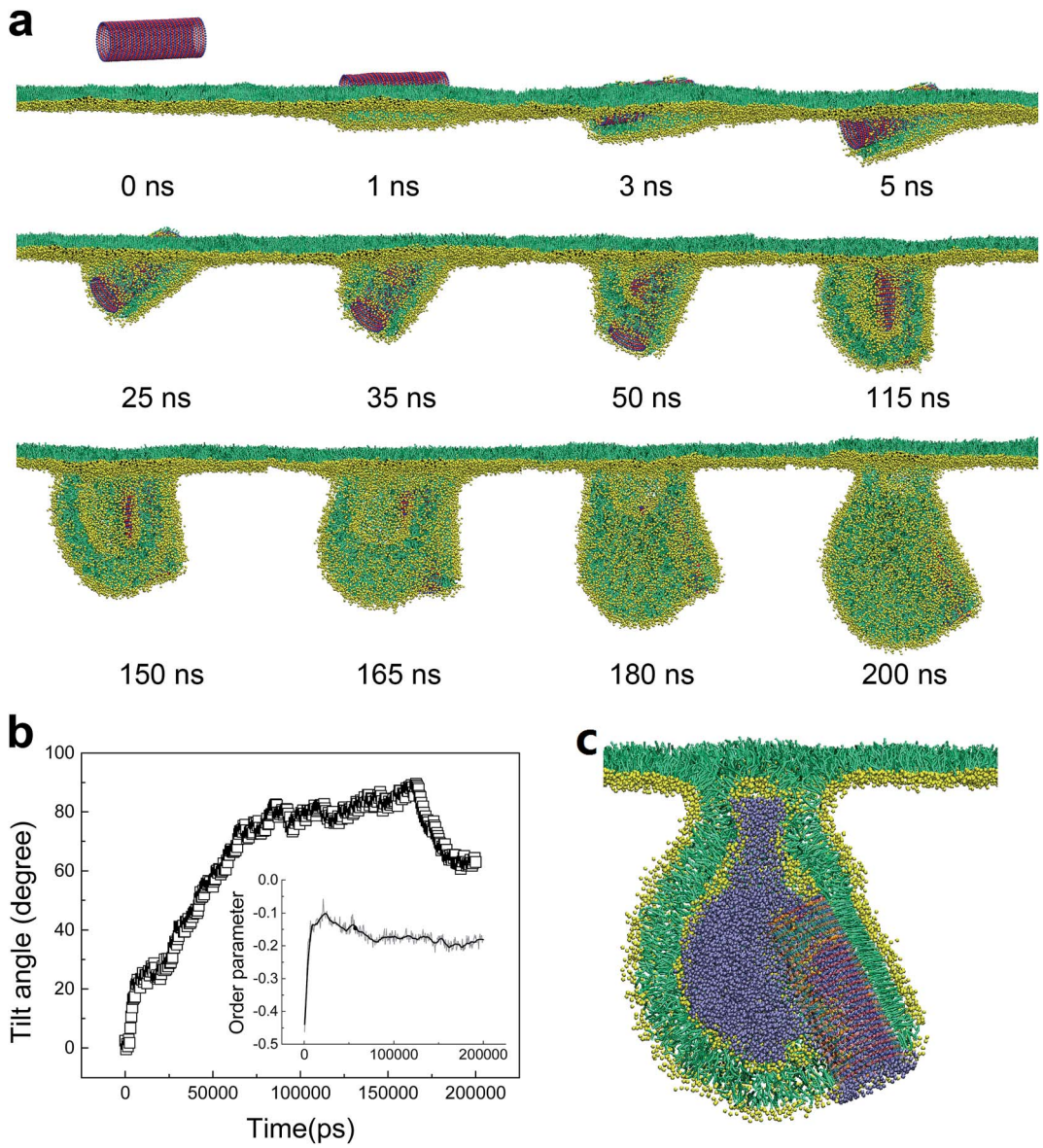

Fig. 8 PSM vesiculation *via* interacting with a SWCNT having 27 tangential pin-stripes. (a) Typical snapshots showing the detailed vesiculation pathway. (b) Time evolution of tilt angle of SWCNT. The inset shows the evolution of order parameter of lipids that adjacent to the tube surface. (c) Cross sectional view of the final configuration where the SWCNT anchored itself into the inner leaflet of the vesicle bilayer. Water molecules inside the vesicle were displayed for clarity.

micelles covering the top hydrophobic surface, like that under expansion condition (Fig. 5a). Under compression, the monolayer bent downwards to wrap the hydrophobic segment, thus dragging the hydrophilic part to get contact with lipid tails and generated unfavorable interactions (Fig. 6b). Shortly, it opened a structural defect from which the translocation occurred *via* a fast tube self-rotating (Fig. 6b inset). As the hydrophobic segment being wrapped by the PSM moved downwards under compression, the hydrophilic segment detached from the PSM, corresponding to a decrease of contact number between hydrophilic tube surface and lipids (Fig. 6b). Finally, the composite reached equilibrium with the steady tube orientation angle of 50° (Fig. 6b, inset). In Fig. 6c, we provide the cross sectional view to illustrate the novel configuration of half wrapping and half translocation. A short bilayer neck was formed to connect the SWCNT with the upper monolayer. The cavity of the hydrophilic segment was filled with water molecules (Fig. 6d), while the inner surface of the hydrophobic segment was attached with lipids by forming an inverse micelle configuration with a small water cluster encapsulated (Fig. 6d and e).

For the SWCNT having four tangential stripes, it followed a similar mechanism interacting with the PSM, but the final configuration was more like a vesicle. We describe in Fig. 7a

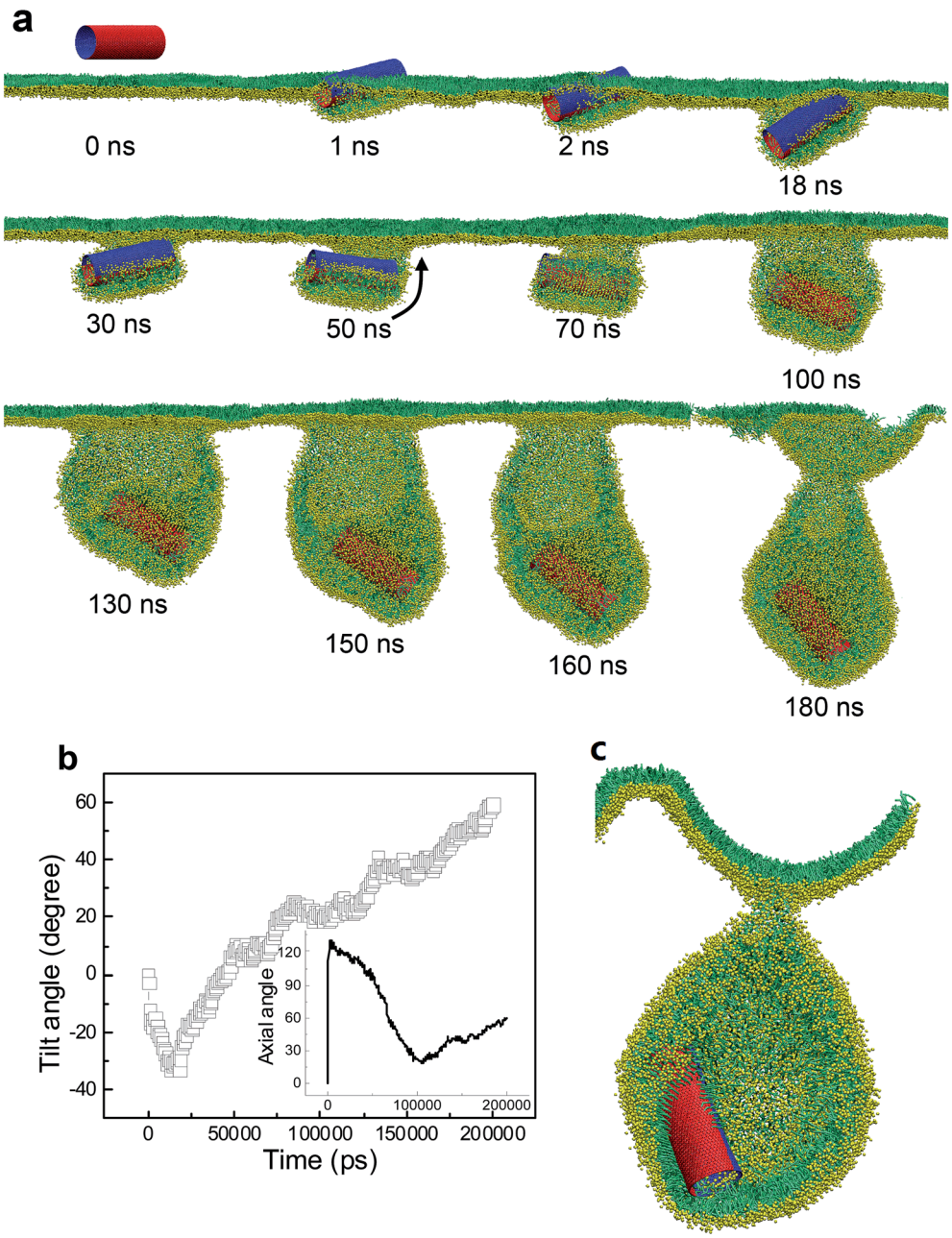

Fig. 9 PSM vesiculation *via* interacting with a SWCNT having two axial stripes. (a) Typical snapshots. (b) Time evolution of tilt angle of SWCNT. (c) Cross sectional view of the final configuration. The rolling behavior was denoted by the black arrow in (a) and further verified by evolution of tube angle along axial direction, given in inset of (b).

a typical simulated vesiculation event of the PSM by interacting with a striped SWCNT. More detailed process can be found in Video S1.† After penetrating through the monolayer, two hydrophilic segments of the SWCNT were immerged in water, while the other two hydrophobic segments were covered by lipids *via* forming two regular ring-like aggregates. Under PSM compression, the lipid aggregates kept protruding and developed into two bilayer patches, which fused with each other to finally construct a vesicle. The time evolution of the orientation angle of SWCNT is given in Fig. 7b. It indicates that the self-rotating of SWCNT can facilitate both early translocation and late bilayer protruding to accomplish the PSM vesiculation. The cross sectional view of the final configuration shows that the SWCNT embedded its hydrophobic segments in two bilayers of the vesicle to stabilize it by playing a role like scaffolding (Fig. 7c).

As we further decreased the stripe width, a different vesiculation pathway was observed (Video S2†). Compared with the

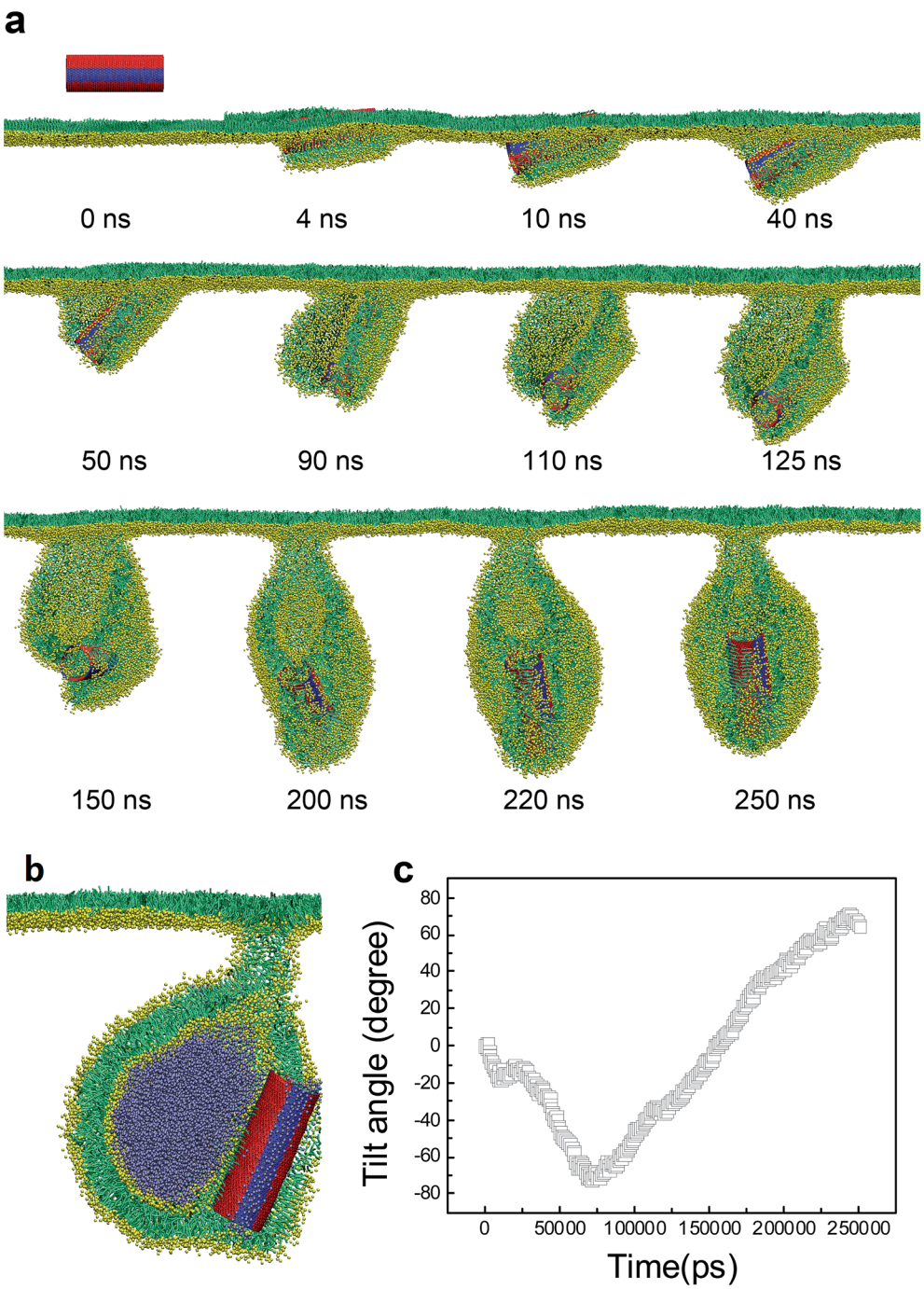

Fig. 10 PSM vesiculation *via* interacting with a SWCNT having six axial stripes. (a) Typical snapshots. (b) Cross sectional view of the final configuration. (c) Time evolution of tilt angle of SWCNT.

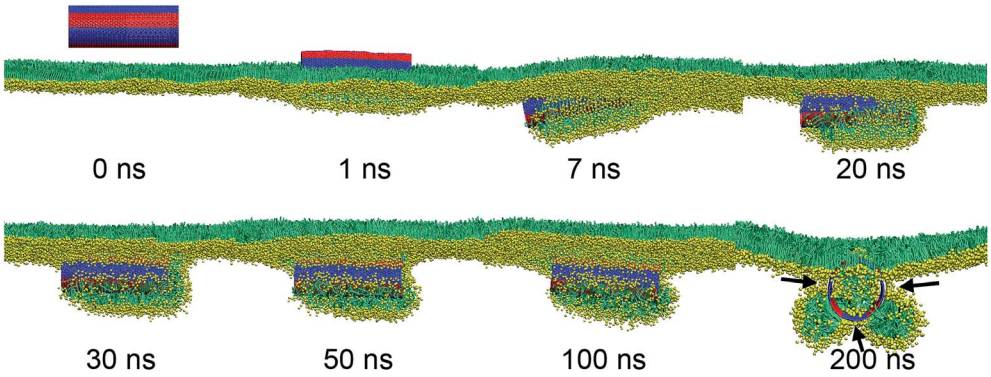

Fig. 11 Failure of PSM vesiculation by interacting with a SWCNT having 8 axial stripes. The shrinking of two bilayer protrusions covering the hydrophobic stripes was denoted by three black arrows.

SWCNTs having wider stripes, the pin-stripe of the SWCNT made it frequent alternating of hydrophobicity along axial direction. This configuration hindered adjacent lipids from forming ordered arrangement adhering on the tube surface. Nevertheless, the first stage of entry followed a wrapping-rotating mechanism (Fig. 8a and b, $t < 75$ ns), which has been observed for pristine SWCNTs and other rod-like NPs (Fig. S2†).[54–56] In the process of tube rotating, two bilayer protrusions appeared, with the SWCNT standing and embedding in the bilayer junction.[57] Under further compression, the two protrusions gradually grew along tube tangential direction and fused to generate a vesicle. Interestingly, by calculating the order parameter of lipids that were adjacent to the SWCNT (Fig. 8b, inset), a self-adjustment of lipid arrangement was observed and expected to facilitate both wrapping and vesiculation. The final vesicle configuration from cross sectional view clearly shows that the vesicle was filled with water molecules and stabilized by embedding the SWCNT into the inner vesicle leaflet (Fig. 8c).

Besides the stripe width, further MD simulations showed equal importance of the stripe orientation of SWCNTs that influences their interactions with the PSM. We look the SWCNT having two axial stripes. To our surprise, it triggered PSM vesiculation (Fig. 9, Video S3†), which was not observed for the SWCNT having two tangential stripes (Fig. 6). Once captured by the PSM, the SWCNT first tilted and behaved as a 'syringe' to penetrate through the PSM (Fig. 9a and b, $t < 18$ ns). Only the hydrophobic side was covered by a lipid aggregate, which was connected *via* a bilayer neck with the upper monolayer (Fig. 9a). Shortly, a reverse rotation towards horizontal orientation was observed to reduce the wrapping asymmetry (Fig. 9b). More interestingly, the covering lipid aggregate was found to grow together with the neck to roll up and encapsulate the SWCNT. The rolling behavior was clarified by evolution of tube angle along its axial direction (Fig. 9b, inset). Finally, a bilayer vesicle was formed with the hydrophobic side of SWCNT anchoring in bilayer and the hydrophilic side facing the inner water phase (Fig. 9c).

To prove the importance of tube rotation, we performed one restrained simulation. The configuration of SWCNT with two axial stripes at $t = 18$ ns was chosen as the initial structure (Fig. S4†). During the simulation the SWCNT was fixed along x and y directions but free along z direction. The aim was to restrain the SWCNT from rotating during translocation. As expected, no vesiculation of the PSM was observed. Instead, the SWCNT kept moving downwards, with the hydrophobic surface being covered by lipids and hydrophilic surface exposed in water (Fig. S4†).

For the SWCNT having six axial stripes, a similar vesiculation event by the mechanism featured with penetrating, rotating and protruding was observed (Fig. 10, Video S4†), confirming the robustness of PSM vesiculation by interacting with the surface patterned SWCNTs. As we further decreased the axial stripe width, surprisingly, no vesiculation was observed (Fig. 11). We ascribe the failure of vesiculation to the negative mismatch between the hydrophobic stripe width and the bilayer thickness. That is the lipid aggregate covering the hydrophobic stripes has to shrink to avoid its contact with adjacent hydrophilic stripes, thus disconnecting it from the upper monolayer. Therefore, further bilayer protruding, which is requisite to vesiculation, was inhibited by cutting off the lipid sources.

At last, we ended our simulations to probe the PSM interaction of SWCNTs having random surface patterning. By varying the ratio of hydrophobicity of SWCNTs, MD simulations showed that PSM vesiculation could occur only by interacting with SWCNTs having lower hydrophobic ratios (Fig. S5†). Both the pathway and the mechanism are similar with that of the pin-striped SWCNTs (Fig. 8), where lipids adjusted their arrangement adhering on the tube surface and formed lipid bilayers, the growth of which finally developed into a vesicle. Higher ratio made it more hydrophobic and thus behaved like a pristine nanotube and was finally wrapped in the folding bilayer (Fig. S6 and 7†).

4. Conclusions

In summary, we have presented the simulation study to uncover the pivotal role of surface patterning of single-walled carbon nanotubes (SWCNTs) interacting with the pulmonary surfactant monolayer (PSM). For SWCNTs having unique surface properties, our simulations revealed direct translocation, vertical insertion, PSM poration and encapsulation events, together with the PSM perturbation that depends on the SWCNT size,

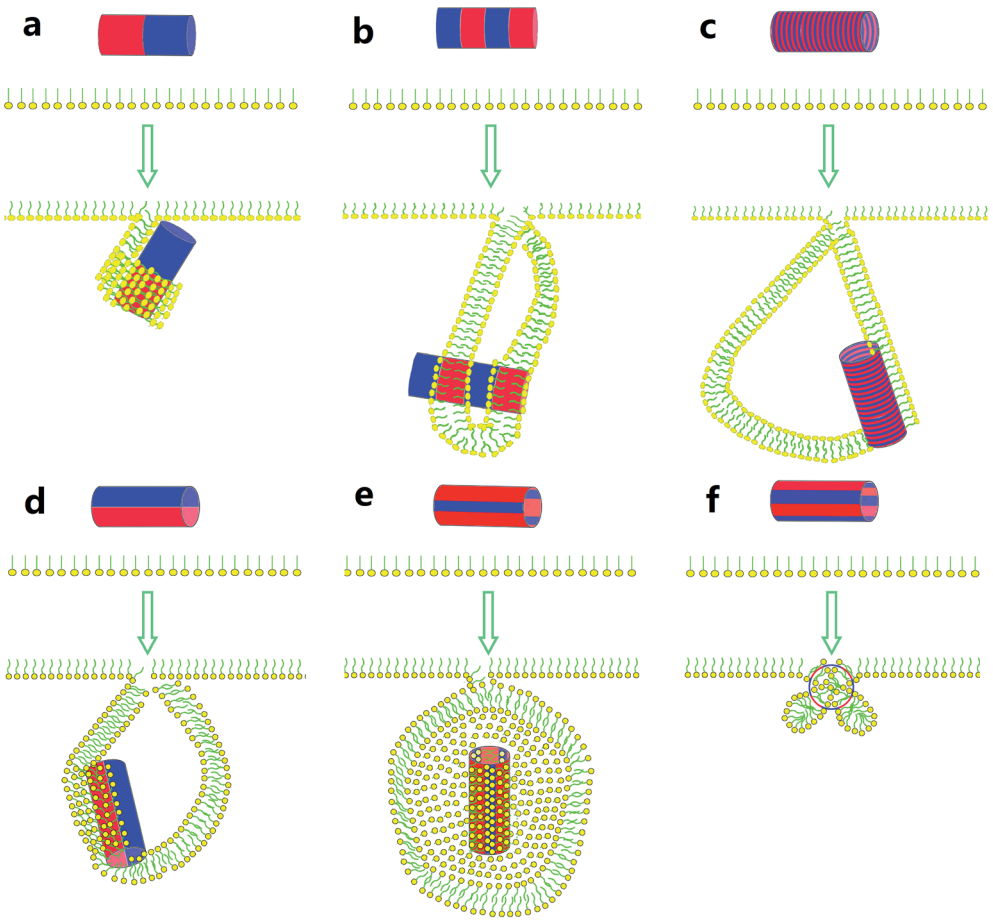

Scheme 1 Summary of the interactions between surface patterned SWCNTs and the PSM under compression, illustrating the importance of both stripe width and stripe orientation.

homogeneous surface hydrophobicity and the PSM tension. For SWCNTs with surface patterning, we observed enhanced PSM perturbation. Under expansion, the PSM translocation was strikingly frustrated *via* inducing ordered or disordered lipid arrangements covering the patterned tube surface. Under compression, the lipid aggregates adjusted themselves to form bilayer protrusions, the growth of which finally developed into vesicles.

As shown in Scheme 1, both stripe width and stripe orientation can influence whether and in what pathway the vesiculation takes place. For the SWCNTs having two tangential stripes, it interacts with the PSM *via* a mechanism that is featured with half wrapping and half translocation (Scheme 1a). Decrease of the stripe width can induce PSM vesiculation and stabilizes it by anchoring the hydrophobic bands in the vesicle bilayer walls (Scheme 1b). Further decrease of the stripe width still triggers vesiculation, yet higher extents of lipid rearrangement and self-adjustment are required (Scheme 1c). For axial striped SWCNTs, only wider stripes could induce vesiculation (Scheme 1d and e). If the hydrophobic stripe width is smaller than the bilayer thickness, the final composite is stabilized by two shrinking micelles adhering on the hydrophobic stripes with no further protruding and vesiculation (Scheme 1f).

Though the regular surface patterning of SWCNTs was found to enhance their penetration through a lipid bilayer[25] and reduce the membrane damage,[23,26] our simulations have revealed an opposite behavior in the monolayer system. That is the PSM perturbation is enhanced by surface patterning of SWCNTs. Apart from the frustrated translocation under expansion, surface patterning of SWCNTs could trigger PSM vesiculation under compression. Both behaviors adversely disturb the organized shape transformation of natural PSM and inhibit its normal biophysical functions. Recent experiments by Valle *et al.* showed that the inhaled carbon nanotubes can induce a concentration-dependent PSM inhibition under physiologically relevant conditions.[58] Our simulations thus provide the molecular view of biophysical inhibition of PSM by inhaled SWCNTs with different surface properties. Therefore, our results can help reveal the inhalation toxicity of SWCNTs and, on the positive side, provide guidelines to design functionalized SWCNTs for use as vehicles in the pulmonary nanodrug delivery.

Acknowledgements

This work was financially supported by National Natural Science foundation of China (no. 21303269), Science and technology major project of Shandong province (no. 2016GSF117033), and Qingdao Science and Technology Project (no. 16-5-1-73-jch).

Simulations were performed at the National Supercomputing Center in Shenzhen.

References

1 E. R. Weibel and J. Gil, *Respir. Physiol.*, 1968, **4**, 42–57.
2 D. Andelman, F. Brochard, C. Knobler and F. Rondelez, in *Micelles, Membranes, Microemulsions, and Monolayers*, eds. W. M. Gelbart, A. Ben-Shaul and D. Roux, Springer New York, New York, NY, 1994, pp. 559–602.
3 A. Gopal and K. Y. C. Lee, *J. Phys. Chem. B*, 2001, **105**, 10348–10354.
4 E. Hatta, *Langmuir*, 2004, **20**, 4059–4063.
5 E. Nikomarov, *Langmuir*, 1990, **6**, 410–414.
6 J. Chayen, *Cell Biochem. Funct.*, 1996, **14**, 75.
7 S. Schürch, R. Qanbar, H. Bachofen and F. Possmayer, *Neonatology*, 1995, **67**(1), 61–76.
8 Y. Y. Zuo, R. A. W. Veldhuizen, A. W. Neumann, N. O. Petersen and F. Possmayer, *Biochim. Biophys. Acta, Biomembr.*, 2008, **1778**, 1947–1977.
9 J. Pérez-Gil, *Biochim. Biophys. Acta, Biomembr.*, 2008, **1778**, 1676–1695.
10 S. Baoukina and D. P. Tieleman, *Biochim. Biophys. Acta, Biomembr.*, 2016, **1858**, 2431–2440.
11 S. Baoukina and D. P. Tieleman, *Biophys. J.*, 2011, **100**, 1678–1687.
12 K. Bhattacharya, F. T. Andón, R. El-Sayed and B. Fadeel, *Adv. Drug Delivery Rev.*, 2013, **65**, 2087–2097.
13 J. P. Ryman-Rasmussen, E. W. Tewksbury, O. R. Moss, M. F. Cesta, B. A. Wong and J. C. Bonner, *Am. J. Respir. Cell Mol. Biol.*, 2009, **40**, 349–358.
14 B. Robertson and H. L. Halliday, *Biochim. Biophys. Acta, Mol. Basis Dis.*, 1998, **1408**, 346–361.
15 P. Avouris, Z. Chen and V. Perebeinos, *Nat. Nanotechnol.*, 2007, **2**, 605–615.
16 R. H. Baughman, A. A. Zakhidov and W. A. de Heer, *Science*, 2002, **297**, 787–792.
17 M. F. De Volder, S. H. Tawfick, R. H. Baughman and A. J. Hart, *Science*, 2013, **339**, 535–539.
18 J. B. Mangum, E. A. Turpin, A. Antao-Menezes, M. F. Cesta, E. Bermudez and J. C. Bonner, *Part. Fibre Toxicol.*, 2006, **3**, 15.
19 K. Bhattacharya, F. T. Andon, R. El-Sayed and B. Fadeel, *Adv. Drug Delivery Rev.*, 2013, **65**, 2087–2097.
20 Z. Liu, S. Tabakman, K. Welsher and H. Dai, *Nano Res.*, 2009, **2**, 85–120.
21 Z. Liu, K. Chen, C. Davis, S. Sherlock, Q. Cao, X. Chen and H. Dai, *Cancer Res.*, 2008, **68**, 6652–6660.
22 Z. Liu, X. Sun, N. Nakayama-Ratchford and H. Dai, *ACS Nano*, 2007, **1**, 50–56.
23 A. Verma, O. Uzun, Y. Hu, Y. Hu, H.-S. Han, N. Watson, S. Chen, D. J. Irvine and F. Stellacci, *Nat. Mater.*, 2008, **7**, 588–595.
24 D. Pantarotto, R. Singh, D. McCarthy, M. Erhardt, J. P. Briand, M. Prato, K. Kostarelos and A. Bianco, *Angew. Chem., Int. Ed.*, 2004, **116**, 5354–5358.
25 S. Pogodin, N. K. Slater and V. A. Baulin, *ACS Nano*, 2011, **5**, 1141–1146.
26 Y. Li, X. Li, Z. Li and H. Gao, *Nanoscale*, 2012, **4**, 3768–3775.
27 S. Rooney, S. Young and C. Mendelson, *FASEB J.*, 1994, **8**, 957–967.
28 M. Frick, S. Eschertzhuber, T. Haller, N. Mair and P. Dietl, *Am. J. Respir. Cell Mol. Biol.*, 2001, **25**, 306–315.
29 A. V. Andreeva, M. A. Kutuzov and T. A. Voyno-Yasenetskaya, *Am. J. Physiol.: Lung Cell. Mol. Physiol.*, 2007, **293**, L259–L271.
30 A. Kaviratna, A. Shah, S. S. Rao and R. Banerjee, *Dyn. Biochem. Process Biotechnol. Mol. Biol.*, 2009, **3**, 21–32.
31 E. Parra, A. Alcaraz, A. Cruz, V. M. Aguilella and J. Pérez-Gil, *Biophys. J.*, 2013, **104**, 146–155.
32 E. Parra, L. H. Moleiro, I. Lopez-Montero, A. Cruz, F. Monroy and J. Perez-Gil, *Biochem. J.*, 2011, **438**, 555–564.
33 C. Vermehren, S. Frokjaer, T. Aurstad and J. Hansen, *Int. J. Pharm.*, 2006, **307**, 89–92.
34 S. L. Duncan and R. G. Larson, *Biophys. J.*, 2008, **94**, 2965–2986.
35 A. V. Titov, P. Král and R. Pearson, *ACS Nano*, 2009, **4**, 229–234.
36 T. Yue, X. Wang, X. Zhang and F. Huang, *RSC Adv.*, 2015, **5**, 30092–30106.
37 M. J. Abraham, T. Murtola, R. Schulz, S. Páll, J. C. Smith, B. Hess and E. Lindahl, *SoftwareX*, 2015, **1–2**, 19–25.
38 S. J. Marrink, H. J. Risselada, S. Yefimov, D. P. Tieleman and A. H. De Vries, *J. Phys. Chem. B*, 2007, **111**, 7812–7824.
39 W. Humphrey, A. Dalke and K. Schulten, *J. Mol. Graphics*, 1996, **14**, 33–38.
40 S. Baoukina, L. Monticelli, S. J. Marrink and D. P. Tieleman, *Langmuir*, 2007, **23**, 12617–12623.
41 Y. Y. Zuo, R. Chen, X. Wang, J. Yang, Z. Policova and A. W. Neumann, *Langmuir*, 2016, **32**, 8501–8506.
42 X. Lin, T. Bai, Y. Y. Zuo and N. Gu, *Nanoscale*, 2014, **6**, 2759–2767.
43 G. Hu, B. Jiao, X. Shi, R. P. Valle, Q. Fan and Y. Y. Zuo, *ACS Nano*, 2013, **7**, 10525–10533.
44 X. Lin, Y. Y. Zuo and N. Gu, *Sci. China Mater.*, 2015, **58**, 28–37.
45 C. F. Lopez, S. O. Nielsen, P. B. Moore and M. L. Klein, *Proc. Natl. Acad. Sci. U. S. A.*, 2004, **101**, 4431–4434.
46 X. Shi, A. von dem Bussche, R. H. Hurt, A. B. Kane and H. Gao, *Nat. Nanotechnol.*, 2011, **6**, 714–719.
47 K. Yang and Y.-Q. Ma, *Nat. Nanotechnol.*, 2010, **5**, 579–583.
48 E. J. Wallace and M. S. Sansom, *Nano Lett.*, 2008, **8**, 2751–2756.
49 M. Lelimousin and M. S. Sansom, *Small*, 2013, **9**, 3639–3646.
50 S. Baoukina, L. Monticelli, H. J. Risselada, S. J. Marrink and D. P. Tieleman, *Proc. Natl. Acad. Sci. U. S. A.*, 2008, **105**, 10803–10808.
51 L. Zhang, M. Becton and X. Wang, *J. Phys. Chem. B*, 2015, **119**, 3786–3794.
52 H.-M. Ding and Y.-Q. Ma, *Nanoscale*, 2012, **4**, 1116–1122.
53 T. Yue, Y. Xu, S. Li, X. Zhang and F. Huang, *Phys. Chem. Chem. Phys.*, 2016, **18**, 18923–18933.
54 C. Huang, Y. Zhang, H. Yuan, H. Gao and S. Zhang, *Nano Lett.*, 2013, **13**, 4546–4550.

55 K. Yang, B. Yuan and Y.-Q. Ma, *Nanoscale*, 2013, **5**, 7998–8006.
56 Y. Li, T. Yue, K. Yang and X. Zhang, *Biomaterials*, 2012, **33**, 4965–4973.
57 J. M. Gardner, M. Deserno and C. F. Abrams, *J. Chem. Phys.*, 2016, **145**, 074901.
58 R. P. Valle, T. Wu and Y. Y. Zuo, *ACS Nano*, 2015, **9**, 5413–5421.